Aerodynamics Gust Response Prediction

Alexis RIGALDO
Department of Aerospace and Vehicle Engineering
Royal Institute of Technology - SE 114 15 Stockholm, Sweden
E-Mail:rigaldo@kth.se

Thesis performed within the Aerodynamic department (Methods and Tools)
Airbus Operations SAS - FR 31060 Toulouse Cedex 09, France

February / July 2011

Abstract

This project presents the work performed within the aerodynamics department of Airbus Operation SAS in Toulouse through a five months master thesis. This department works with the industrialization and the use of tools developed by laboratories to perform CFD aerodynamic simulations. The primary purpose of the present work was to support the development of gust analysis methods based on CFD. A new gust model has been developed and integrated to the aerodynamic solver elsA. This solver has been used in order to compute the unsteady aerodynamic simulations for both gust loads and forced motions with CFD. The results were then compared with those from a Doublet Lattice Method computation for validation. Once the validation phase was ended with good agreement between the two methods, a Chimera simulation has been carried out.

Nomenclature

α	=	angle of attack ($^\circ$)
D	=	drag (N)
L	=	lift (N)
M	=	pitch moment (N)
C_D	=	drag coefficient
C_L	=	lift coefficient
C_m	=	pitch angle coefficient
W	=	weight (N)
V	=	velocity ($m.s^{-1}$)
M	=	Mach number (N)
m	=	mass of the aircraft (m)
g	=	Standard gravity ($m.s^{-2}$)
q	=	dynamic pressure (Pa)
M	=	Mach number
S_{ref}	=	reference area (m^2)
b	=	span (m)
c	=	reference chord (m)
k_h	=	spring stiffness in plunge ($N.m^{-1}$)
k_α	=	spring stiffness in pitch (N)
J	=	mass moment of inertia ($kg.m^2$)
w_g	=	gust velocity ($m.s^{-1}$)
L_g	=	gust length (m)

Introduction

Aircraft design has to ensure sufficient strength in the structure to survive atmospheric turbulences. Thus, the gust response is of uttermost importance for the dimensioning of the aircraft. Mathematical specifications of turbulences have been developed and are used in the design process. The successful researches in numerical simulations made during the last years for the unsteady aerodynamic prediction offer now the opportunity to simulate the gust response on an aircraft with complex CFD. Basic gust models are used here on diverse configurations in order to perform simulations with elsA software and to validate the implemented gust code. The work on post processing is also presented with the different tools used after computation. DLM is the actual industrial method used in Airbus for gust response and load calculations. The results of this method are important for comparison with URANS simulations and validation of the CFD model. Chimera simulations, on the HiReTT configuration with aileron, are also computed for application of the method on an industrial configuration.

1 Theory

1.1 Used software and tools

A CFD solver, named elsA and developed in collaboration by the ONERA and the CERFACS, is used in order to perform the simulations and computations. This software is a structured multiblock solver. It solves the compressible, three-dimensional Reynolds Average Navier-Stokes (RANS) equations in a cell centered finite volume formulation from low subsonic to high supersonic regimes. A large variety of turbulent models are available and several matching techniques are developed for multi-block structured meshes in order to perform calculations on complex configurations.

Calculation process

Two types of simulations are performed through the validation process: steady and unsteady simulations.

In order to run a computation through elsA, the user has to provide some geometrical data (mesh coordinates), topological data (connectivity between blocks), physical data, and boundary conditions. Here, a DAMAS database (*.sda), defining the geometry and the mesh of the problem, and a calculation file (*.don), defining the elsA parameters for the calculation (numerical parameters, boundary and initial conditions, the machine in which calculations will be run, the number of processors used, etc.) are used as input. ElsA can run calculations in parallel. Each processor, used during the computation, is responsible for the computation of some blocks only. For each run, elsA generates an information file with warnings and errors if any. More details about elsA and its implementation are available in a tutorial on the Onera website [1].

A steady simulation is performed before any computations in unsteady conditions. ENS++, an Airbus program, is then used for the post-processing in Euler and Navier-Stokes computations. Local quantities (Mach, pressure, etc.) can be extracted or global quantities (lift, drag, mass flow, residuals, etc.) calculated. The interface xmrg is used to show the computed variables in a plot and to compare the results. For the unsteady simulations process, the results from the steady case are used and represent the initial state. The damas database is modified and the model deformation is included. The model defines each node displacement in the mesh calculated by the mesh deformation method developed in reference [2] based on a combination of the analytic method and the Trans-Finite Interpolation (TFI).

1.2 Basic gust studies

The nature of the gust field is reduced to a one dimensional discrete gust with some specific shape definition. The second approach is to look for the harmonic response by introducing a sinusoidal function. For both methods, a set of gust velocities for specific flight conditions have been defined.

Gust models are defined as velocity fields with specific form and amplitude, initial position, direction, wavelength, velocity and direction of propagation. When the gust arrives on the profile, there is a modification of the angle of attack and thus a perturbation of the flow over the profile. Two main gust models are used: the model "1-cos" and the model "sharp edged", and both shapes are shown in figure 1. For comparison with the actual industrial method for gust simulations, harmonic gusts are preferred. The simplest model is the sharp edged gust model compare to the cosine gust which is more elaborated. Both of these are deterministic. The sharp edged gust model represents a wind gust that results in an instantaneous change in direction of the flow and is defined by equation 1. Although this case leads generally to overestimate the gust loads, it is used to validate the gust model. This deterministic analysis is also used in various cases in aircraft design for sudden changes in the relative flow circulating over the aircraft's lifting surfaces in order to get some useful insight about the trajectory deviation and the elastic deformations. The one minus cosine gust model can be generated by a mountainous terrain for example and is defined by equation 2.

$$w_g(x) = \begin{cases} 0 & ,x < 0 \; and \; x > L_g \\ w_{g0} & ,x \in [0, L_g] \end{cases} \quad (1)$$

$$w_g(x) = w_{g0}(1 - cos\frac{2\pi x}{L_g}),\ 0 \leq x \leq L_g \quad (2)$$

where x is the position of the aircraft, w_g the temporal variation of the gust velocity, w_{g0} the maximal value of the gust velocity, and L_g the gust length.

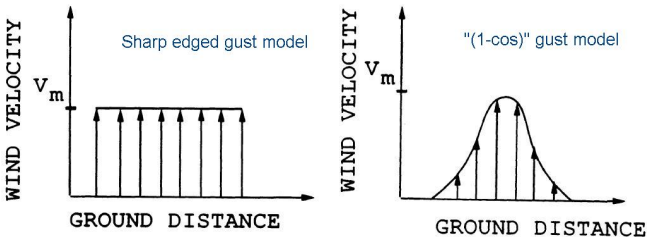

Figure 1: Gust's models, from [3]

An important assumption is that the shape of the gust is not affected by the presence of the body.

1.3 Flight conditions and structural models

Simulations are performed in subsonic and transonic flows. The unsteady CFD simulations are performed on an airfoil profile and then on a three-dimensional aircraft model. The airfoil is represented by a symmetric NACA 64A10 profile. The three-dimensional case is represented by a mesh built from previous efforts in the HiReTT project which is a structured multiblock mesh with 19 blocks, more than 3.6 millions nodes and around 110 surfaces. It represents a fuselage of 70.4 meter long and a half-wingspan of 39.5 meters. Figures 2 and 3 are showing the meshed surfaces of the NACA 64A10[1] and the HiReTT models. Usual flight conditions are considered and parameters are shown in table 1. The upstream boundary is situated at $140.8m$ from the nose of the HiReTT configuration. These values are set by the aerodynamics department.

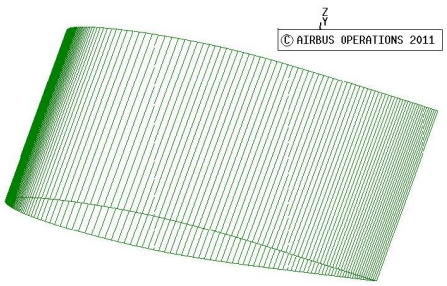

Figure 2: NACA 64A10 model

[1] two dimensional profile, two blocks, 81092 nodes

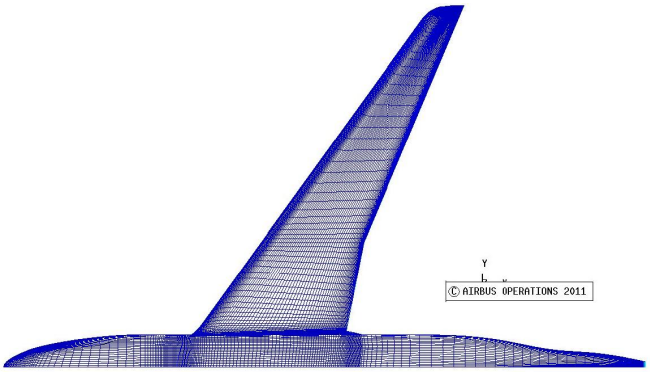

Figure 3: HiReTT model

Aerodynamic parameters		
	NACA 64A10	*HiReTT*
Mach	0.796	0.85
Angle of attack α	-0.21°	1°
Sideslipe angle β	–	0°
Reynolds number	13.0e6	1.825e6
Turbulence rate	1%	1%

Table 1: Aerodynamic parameters for computation

Adjustment of simulations parameters

As explained previously, a steady computation is used to initialize the unsteady computation. The steady computation has been performed with a multigrid scheme in order to get a quick convergence. The unsteady simulation is then performed with the propagation of a gust model. The evolution of the different parameters along the time is recorded by elsA and then plotted. Some of these results are shown in the following sections.

After computations and using the flight conditions defined previously in table 1, the elsA software gives a steady solution of the Navier-Stokes equations after 500 multigrid cycles. In steady simulation, the lift coefficient is $C_L = -4.45 * 10^{-2}$ with the same conditions.

Dual time stepping convergence

The dual time stepping is used to ensure a second order time accuracy when the steady sub-iterations converge. A maximum number of iteration N_{max} and a convergence criterion have been fixed in order to get an accurate solution with the lowest amount of CPU time possible. From previous computations and analysis done in the department, a dual time step of fifty gives a completely converged solution.

The value of ten for the dual time step has been chosen after computations and analysis for the NACA64A10 test case. More information are presented in section 2. The maximal error with a value of 10 is, for the drag coefficient point of view, less than 0.13% and this accuracy is sufficient in order to perform the different validations in this project. This does not give error for the moment and lift coefficients. Concerning the HiReTT simulations, the chosen time step is 25.

Harmonic signal characteristics

For a harmonic signal, the relation between the number of steps $N_{step,0}$ in one period, the frequency of the oscillation f and the time step Δt is defined in equation 3.

$$N_{step,0} = \frac{1}{\Delta t * f} \tag{3}$$

From the propagation gust velocity v_{prop} and the gust wavelength λ, the frequency of the signal is computed

$$f = \frac{v_{prop}}{\lambda} \tag{4}$$

1.4 Test of the gust response simulations

The aircraft generates aerodynamic forces by means to its velocity relatively to the surrounding air. Thus, a sudden change in the velocity of the surrounding air, caused for example by the presence of a wind gust, or in wind direction, introduces a change in these aerodynamic forces.

1.4.1 Rigid and static models

Solutions are obtained with undeflected rigid profiles. The rigid wing has a greatest lift than its aeroelastic model and highest lift-to-drag ratio. Nevertheless, the main purpose of this paper is to validate a gust model and thus, if only rigid models are used for computation and theory, this difference is not important. The models are considered to be static. Only the surrounded flow is moving over the profile in the same manner as done during a wind tunnel analysis.

1.4.2 Dynamic models

An aircraft, or a wing, is a dynamic structure which is allowed to move. This section presents the computations performed on dynamic models. A simple two dimensional dynamic model of the NACA64A10 airfoil section is considered. The airfoil section geometry is shown in figure 4 and the data are defined in section 2.2. The length of reference for the NACA64A10 airfoil profile is $1m$ and for the HiReTT configuration is $11.507m$.

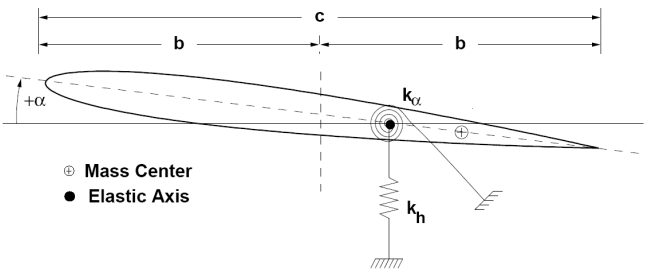

Figure 4: Geometry for typical two-Degree-of-Freedom (2-DOFs) airfoil profile model (from [4])

The structure consists of a rigid airfoil section of which the motion is restrained by two linear springs. The section has thus two degrees of freedom that define its motion: a vertical translation $h(t)$ (plunging) and a rotation $\alpha(t)$ (pitching) around its elastic axis. Springs' stiffness k_h and k_α give a horizontal equilibrium at $h = \alpha = 0$. The section has a mass m and a mass moment of inertia about the centre of mass J. The considered model undergoes forced oscillations due to the gust excitation. The differential equation system describing the motion of the structure is written in equation 5 with S_α, I_α, respectively the static and the inertia momentum around the elastic axis.

$$\begin{cases} m\ddot{h} + S_\alpha\ddot{\alpha} + k_h h = -\mathcal{L} \\ S_\alpha\ddot{h} + I_\alpha\ddot{\alpha} + k_\alpha\alpha = -\mathcal{M} \end{cases} \tag{5}$$

Small amplitude motions of the structure around the steady state equilibrium are considered. Under these assumptions, the use of linear structural dynamics simplifies the aeroelastic analysis and leads to a fairly good estimate of the structure behaviour. Thus, introducing a structural stiffness matrix $\mathbf{K}$, relating the incremental structural deformation to the incremental elastic restoring forces, and a constant mass matrix $\mathbf{M}$, relating the structural acceleration to inertial forces, the linear time domain equations of motion may be written:

$$\mathbf{M}\ddot{\mathbf{q}} + \mathbf{K}\mathbf{q} = \mathbf{F}_{aero}(t, \mathbf{q}, \ddot{\mathbf{q}}, ...) \tag{6}$$

where the right and the left hand sides represent respectively the internal and the external forces, $\mathbf{q}(t) = [h(t)\ \alpha(t)]^T$ is the displacement vector. The mass and structural stiffness matrices are defined by equation 7.

$$\mathbf{M} = \begin{bmatrix} m & -ms \\ -ms & J \end{bmatrix} \quad \text{and} \quad \mathbf{K} = \begin{bmatrix} k_h & 0 \\ 0 & k_\alpha \end{bmatrix} \tag{7}$$

The global equation of motion without aerodynamic forces is now considered in order to set the airfoil structural properties. For simplicity, the case when s=0 is considered, giving two decoupled linear systems with eigenfrequencies:

$$\omega_1 = \sqrt{k_h/m} \quad \text{and} \quad \omega_2 = \sqrt{k_\alpha/J} \tag{8}$$

From the rigid simulations, and the desired maximum displacement δ_h and δ_α, the springs' stiffness k_h and k_α are calculated with the following formula:

$$k_h = L_i/\delta_h \quad \text{and} \quad k_\alpha = M_i/\delta_\alpha \tag{9}$$

L_i and M_i are two chosen values of lift force and pitching moment around the rotational axis. With a fixed time step Δt, a period of oscillation $T_i = 2\pi/\omega_i$, and the choice of a number of thirty points per period to build the gust response ($\frac{T}{\Delta t} \geq 30$), the mass and mass moment of inertia are defined using the following equations:

$$m \geq \left(\tfrac{30\Delta t}{2\pi}\right)^2 k_h \quad \text{and} \quad J \geq \left(\tfrac{30\Delta t}{2\pi}\right)^2 k_\alpha \tag{10}$$

In the same way, a dynamic model of the HiReTT configuration is build in order to simulate the response of the structure.

1.5 Comparison with DLM method and validation of the gust response

Most of the Airbus department, performing aerodynamic gust responses, use a planar Doublet-Lattice Method (DLM) to compute oscillatory aerodynamic analysis and the gust responses. This method is based on a three dimensional unsteady linearized potential flow. Lifting surfaces are approximated to flat and thin plates. The method allows the computation of the lift distribution on oscillating surfaces in subsonic flows. It is derived from the linearized formulation of the oscillatory subsonic lifting surface theory which is described in reference [2]. The DLM methods are used today for their cheapness but they cannot be used for transonic flow.

The three dimensional shape of the wing is restricted to a set of panels. Each cell of the mesh contains an approximation of the pressure differences between the upper and the lower surface of the wing. The aerodynamic effects due to the wing thickness are not taken into account. Navier Stokes Unsteady simulations with elsA have been shown to be efficient enough to get a correct prediction of the unsteady aerodynamic loads in reference [2]: boundary layers and non linearities are simulated. Nevertheless these methods are very expensive.

Comparisons between DLM methods and CFD computations have been performed. Two types of simulations are compared here. The first one is with gust propagation and the second one is with forced motion. In both cases the motion will be harmonic, at least after a transition period between a steady state and a permanent oscillatory motion.

Aerodynamics problems are, in general non-linear, and the responses to a harmonic signal at a precise excitation frequency are not necessarily at the same frequency. However, the unsteady simulations are limited to small forced mesh displacement and thus a linear approach can be justified. In such a physical system, the response to a harmonic excitation is a harmonic signal at the same frequency and with a certain gain in amplitude and a phase shift. After a short transient period, the flow response becomes periodic in time. The post-processing consists in analysing this periodic response. The different physical values can be decomposed in Fourier series and particularly the pressure coefficient C_p is given by equation 11. Only the more important harmonic for the response validation appears in this equation. It is the first harmonic.

$$C_p = \overline{C_p} + A[Re(C_p)\cos(\omega t) + Im(C_p)\sin(\omega t)] \tag{11}$$

where $\overline{C_p}$, $Re(C_p)$ and $Im(C_p)$ are respectively the pressure coefficient mean term, the real and the imaginary terms; A is the mode amplitude of the unsteady simulation. The reduced frequency of the excitation is defined by the following equation 12 where c is the chord, ω the pulsation and V the velocity.

$$k = \frac{c.\omega}{V} \tag{12}$$

The C_p distribution is considered for all the physical time step computed. For the validation of the unsteady

simulations performed with elsA, the comparison of the C_p average value and its first harmonic is done with DLM data. With a post-processing on a single period, the value of the first harmonic is calculated. This first harmonic is a complex value and comparisons have to be done on both real and imaginary parts.

ENS++ is then used for the post-processing in Navier-Stokes computations to extract the calculated values. A MATLAB code has been developed in order to perform a comparison between the different methods. An extrapolation from the FFT outputs: $Re(C_p)$ and $Im(C_p)$, on the upper and lower surface is used in order to get the values $\Delta Re(C_p)$ and $\Delta Im(C_p)$.

1.6 Application: Chimera technique simulation

Unsteady CFD Chimera simulations are performed on the HiReTT configuration. The configuration used in the previous sections is implemented with a movable aileron. This configuration is equivalent to an Airbus A380. The single flight condition used is this one set for the HiReTT configuration in table 6 in section 2.3.2. Firstly a steady simulation is performed for two configurations: one with a zero degree aileron deflection and one for a five degrees deflection. The mesh is shown is figure 5.

The mesh is constituted by 251 blocks, 14273723 nodes and 2476290 cells. The aileron is situated at 73% of the half wing span from the middle of the fuselage and is 9.038 meters long. The lateral distance between the movable aileron and the fixed wing is quite small: $75mm$ for an $80m$ wingspan aircraft, as figure 6 shows. In these holes, the mesh is refined in order to simulate the particular phenomena that could occur for the airflow in this region. When the aileron displacement is imposed, the mesh is deformed in order to adapt the different elements to the new configuration. Figure 6 shows the aileron and its deflection.

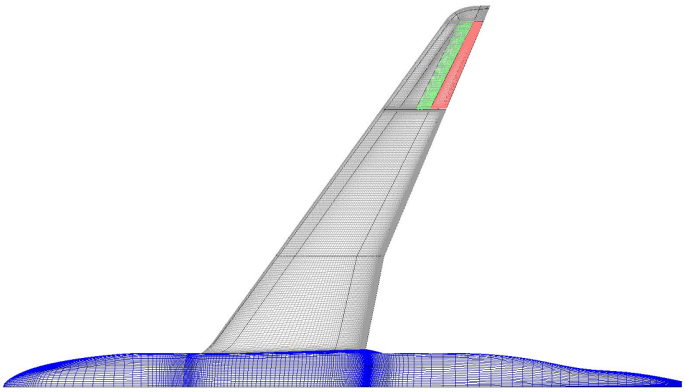

Figure 5: Surface mesh of the configuration

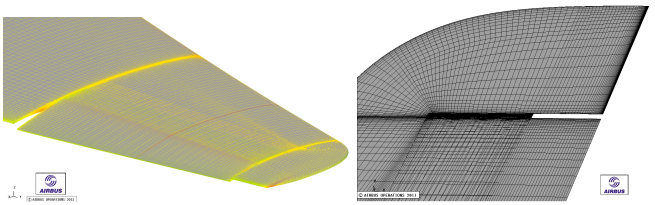

Figure 6: Movable aileron with hole and details at the wing tip

2 Results

One feature of the gust response of an aircraft, or of a lifting surface, that can be studied is the variation in the response as the gust shape and length are altered. DLM are used today for gust response studies in Airbus. Results from the comparison between CFD and DLM are presented here. In the last subsection, Chimera simulations results are shown for an application to an industrial configuration.

2.1 Rigid and static models

2.1.1 Rigid motion of an airfoil section

Results are presented here for a gust turbulence felt by the NACA 64A10 airfoil. In this configuration, the steady computation has been performed without highlighting any problem. The initial angle of attack is negative and thus the lift coefficient is non zero in steady flow.

Physical time step influence

The unsteady simulation has been simulated with 10, 20, 30 and 50 time steps per cycle. The value of 10, for the dual time stepping, is enough to get converged in lift. Nevertheless when the drag coefficient is studied, a time step of 10 gives some differences with the 50 time steps' results. The maximal error with a value of 10 is, for the drag coefficient point of view, less than 0.13% and this accuracy is sufficient for these simulations. This value gives also a lower computational time. The study on the time step has been performed with the parameters defined in table 1.

Discrete gust response

At first, a discrete "1-cos" gust response is studied. In this section you may find figures showing the evolution of the lift and pitch moment coefficients with time. The abscissa represents a number of steps and has to be modified in order to get the real time evolution. A modification in gust amplitude is performed. Figure 18 shows that the amplitude of the response is increasing in the same way than the amplitude of the gust. When the gust arrives, the angle of attack is modified and thus the lift increases. For higher gust amplitudes, the modification in the local angle of attack is greater and thus the maximum lift coefficient endured by the wing grows.

Then, a discrete "sharp edged" gust profile is chosen. An increase in gust's amplitude introduces an increase of the lift coefficient as it is shown in figure 19. The pressure is growing and the displacement amplified.

Harmonic gust response

Before looking at the influence of the different gust parameters on the response, the permanent state is studied in the case of a harmonic gust response. After 1500 iterations in unsteady simulation (so without taking into account the 500 iterations in steady simulation), the system has converged towards a permanent oscillatory state, in the case of $\alpha = -0.21°$.

Figure 20 shows that when the amplitude of the gust increases, the harmonic responses have the same type of pattern. After a transient period, the lift coefficient of the airfoil tends to a permanent oscillatory state and oscillates around a higher lift coefficient value when the amplitude of the gust is increased. For very high gust wavelength, the response wioll come back to the initial value before increasing again at each period. The oscillation does not occur around a zero lift value and this is due to a non zero angle of attack, and a too short gust wavelength.

2.1.2 Rigid motion of the HiReTT configuration

The first step is to perform a steady simulation and then to begin the unsteady simulations from this steady case in the same way as already performed for the NACA 64A10 profile.

For the steady computation, two test cases are performed: one with attached flow (angle of attack $\alpha = 1°$) and one for separated flow (angle of attack $\alpha = 3°$). The convergence of these steady computations is an indicator for the prediction of Dual Time Step inner loop convergence. A poor convergence may highlight some problems in the mesh or in the numerical methods. The elsA software get a steady solution of the Navier-Stokes equations in 400 multigrid cycles for the case with attached flow and $\alpha = 1°$, and in 900 multigrid cycles with separated flow and $\alpha = 3°$.

The unsteady simulation has been simulated with 10, 15, 20 and 50 dual time steps per cycle. The value of 10, for the dual time stepping, is enough to get a convergence in lift. Nevertheless when the drag coefficient is studied, a time step of 10 gives some differences in the convergence with a maximum error of 1.29% compare to the results with a fifty dual time steps. A time step of 20 gives less than 1% percent error and is used here.

Discrete gust response

For the discrete response, the computations have been performed with a variation in gust amplitude. After 500 steady iterations, the unsteady simulation starts. When the gust encounters the nose of the aircraft the lift increases. Then, when the gust arrives on the wing, the increase is faster and the generated a higher lift than the body one since the wing is designed to generate lift with a large wetted area. Once the wing is not anymore under the influence of the discrete gust, the lift coefficient decrease and come back to its initial value as it is seen in figure 21.

Lift coefficient variation with α_{gust}

The linearity of gust response with the excitation is one the first things to look at before validation. The linearity allows extrapolation of values when performing gust simulations. After some unsteady computations, it has been shown that the lift coefficient undergone by the HiReTT configuration ($\Delta C_L = C_{L,final} - C_{L,inital}$) varies linearly with the gust excitation $\Delta\alpha_{gust}$. This pattern is shown in figure 7. Equation 13 gives the definition of α_{gust}.

$$\tan(\alpha_{gust}) = \frac{gust\ velocity}{propagation\ velocity} \tag{13}$$

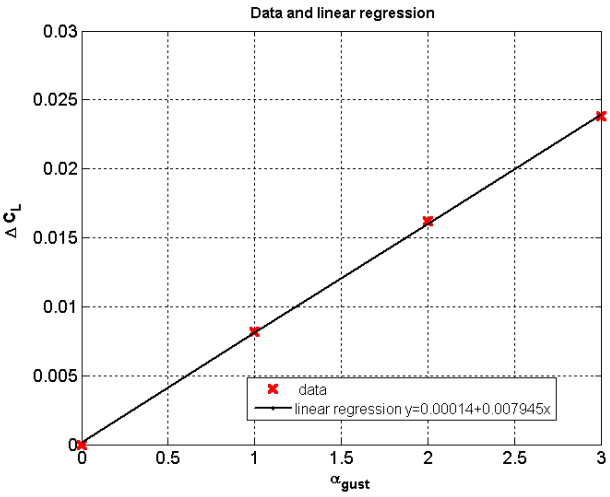

Figure 7: Lift coefficient variation with α_{gust}

Harmonic gust response

For the harmonic response, the computation has been performed with the help of gust amplitude variation. Figure 22 shows an increase in lift coefficient as well as in roll and pitch moment, in absolute value, when the angle α_{gust} is increasing (higher gust velocity).

2.2 Dynamic models

Dynamic simulations are launched essentially in order to see if the gust model is running with dynamic motion. The load factor is computed and compared to the theoretical values from the EGL (Aerodynamic loads) department.

2.2.1 Dynamic simulations' parameters

The tables 2 and 3 give the structural parameters for the dynamic simulations. For each models, a mass, a mass moment of inertia and springs' stiffness are defined.

Movies can be created with models' snapshots from quick-view software. They show the evolution of the pressure on the skin of the model.

Translation	mass m	stiffness k_h
h	$1 * 10^{-4}$	3
Rotation	inertia I_α	stiffness k_α
α	$1 * 10^{-3}$	20
Translation	vector	(0,0,0.01)
Rotation	point	(0.248,-0.5,0)
	vector	(0,1,0)
	angle	1.01

Table 2: Structural data for the NACA airfoil

Translation	mass m	stiffness k_h
h	$5.20 * 10^1$	2.302
Rotation	inertia I_α	stiffness k_α
α	$8.81944 * 10^2$	$3.913 * 10^1$
Translation	vector	(0,0,0.01)
Rotation	point	(27000,0,0)
	vector	(0,1,0)
	angle	1.01

Table 3: Structural data for the HiReTT configuration

2.2.2 Load factor

The theoretical load factor Δn_{se} for a sharp-edged gust profile is given by equation 14 (from [5]). The experimental load factor is calculated with equation 15 from the acceleration in plunge given in output after computations.

$$\Delta n_{se} = \frac{\rho U_0 V C_{L\alpha}}{2W/S} \tag{14}$$

$$\Delta n = \frac{\ddot{h}}{g} \tag{15}$$

These equations are used in order to estimate the gust loads in a first approximation. Usually, the value is over-estimated with the theoretical formula and needs to be confronted to other estimated values from some different computational methods. The loads undergone by the wing profile for different gust amplitude have been studied and compared to the theoretical results. Results are presented in the table 4. The error is around 13.5% for each value.

Gust angle α_g	Theory ($*10^5$)	Experiment($*10^5$)
0.5	1.754	1.517
1	3.509	3.010
1.5	5.264	4.552
2	7.019	6.063

Table 4: Loads on NACA64A10 for gust simulation

2.3 Validation with DLM

2.3.1 NACA64A10 wing profile

Gust response

The comparison between DLM and CFD computations is performed with different gust wavelengths $L_{g,i}$: 71.97, 35.90, 18.00 and 7.17. The DLM gives the pressure difference across the surface. The simulations are run with a small gust velocity in order to stay in the linear region found previously in section 2.1.1: $\alpha_g \in [0°, 3°]$ in this paper. The results plotted are always adimensionalized by the gust velocity and thus can be compared between us. The gust propagates at a Mach number of $Ma_\infty = 0.5$. The temperature is $273K$ and the altitude is $2330m$ which gives a Reynolds number of $Re = 9.708 * 10^6$. The initial angle of attack α is 0° for these simulations.

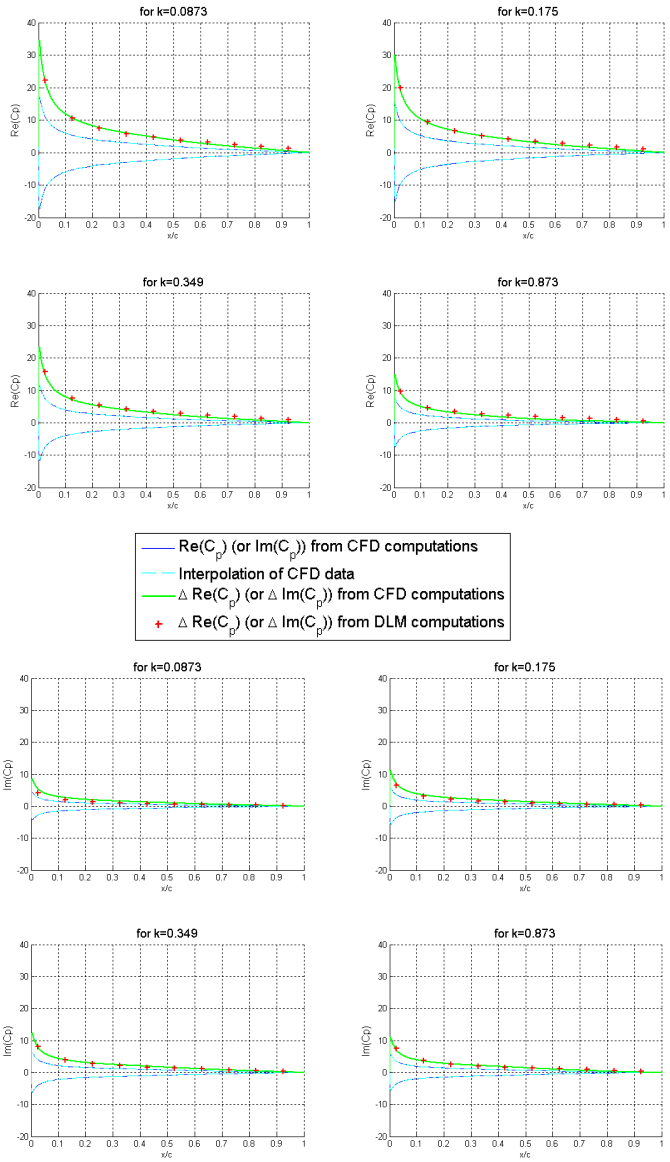

Figure 8: Comparison between CFD and DLM data for $Ma = 0.5$ (gust response)

The numerical results were thus obtained for various values of reduced frequencies k_i: 0.0873, 0.175, 0.349,

and 0.873, calculated with equation 12. The results are presented in figure 8 for the real and imaginary parts of the oscillatory pressure coefficient difference (first harmonic). For a transonic simulation, the DLM cannot be used anymore. A CFD simulation has been performed at Mach 0.8 for comparison with the simulations in subsonic flow (Mach 0.5 here). Results are shown in figure 9.

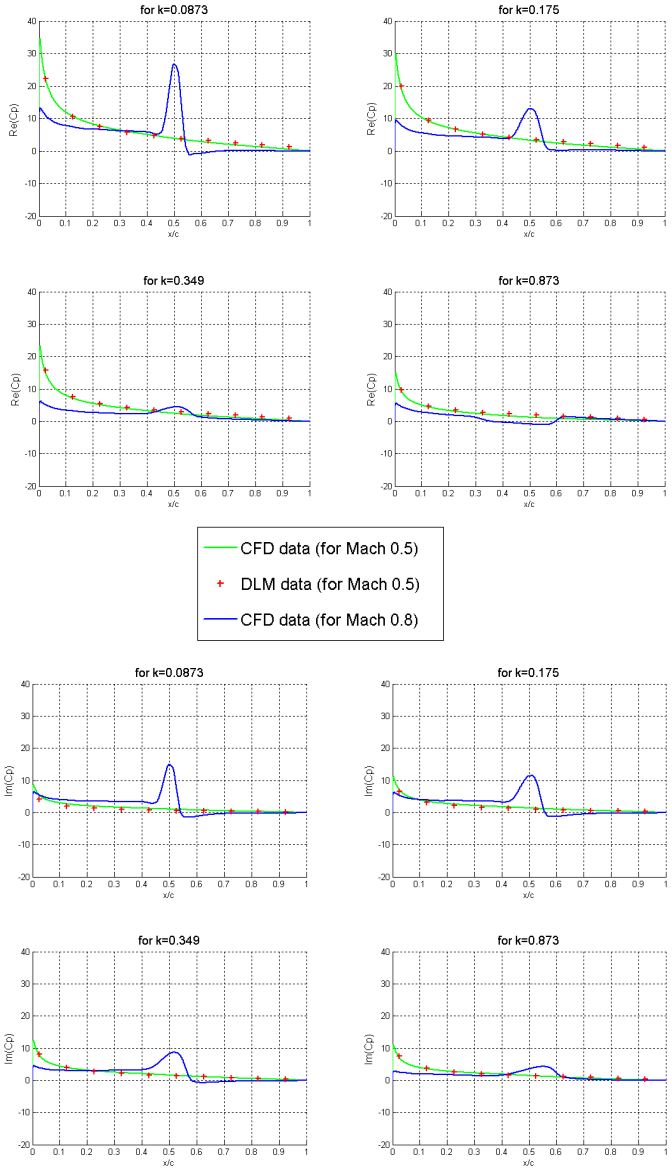

Figure 9: Comparison between two different mach numbers for CFD computations

Forced motion

For the unsteady simulations, a forced motion in translation is imposed on the skin of the airfoil profile. The vertical translation amplitude is set to $h = 0.1m$ and the same reduced frequencies as the gust simulations are used: $k \in [0.0873; 0.175; 0.349; 0.873]$. The vertical oscillatory translation $h(t)$ is expressed as:

$$h(t) = h\exp(i\omega t) \tag{16}$$

Where ω and t are respectively the frequency and the time. The same flight conditions are used than for the gust response. The Reynolds number per meter is $9707577m^{-1}$.

Mach	C_L	**Altitude (m)**	α (°)	**T(K)**
0.5	0.3	2330	0	273

Table 5: Initial conditions

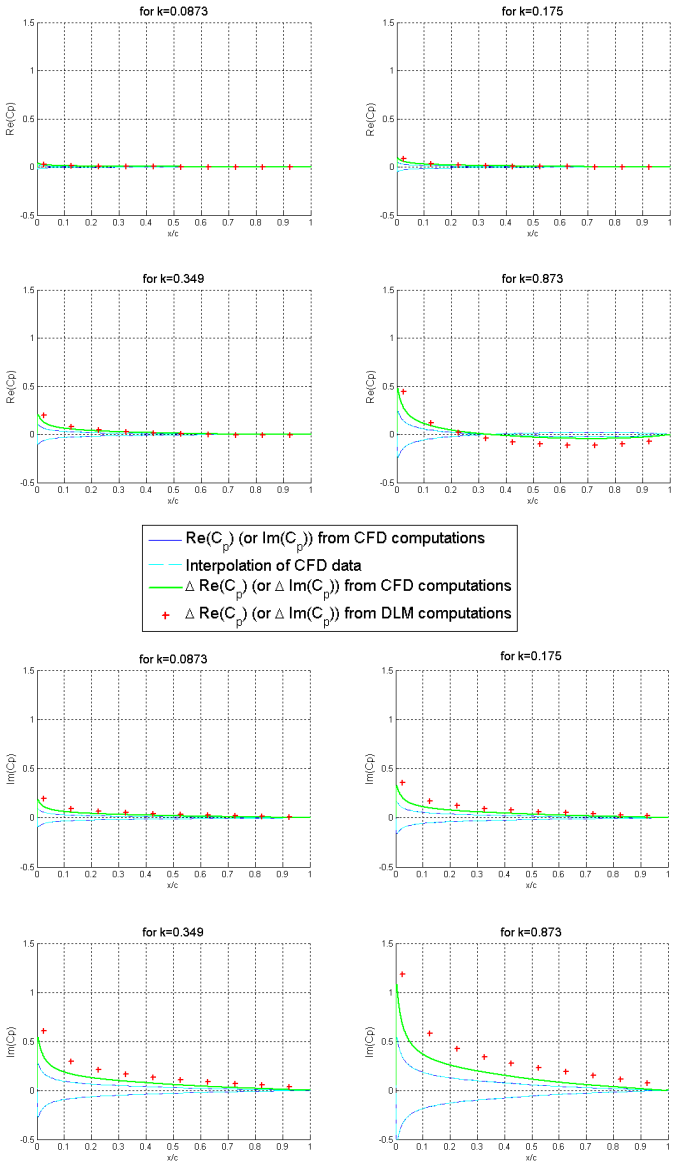

Figure 10: Comparison between CFD and DLM in forced motion ($Ma = 0.5$)

2.3.2 HiReTT configuration

In the case of the HiReTT configuration, a comparison between the two methods (DLM and CFD) has been also done. Two reduced frequencies k_i are chosen: 0.01 and 0.1 which correspond respectively to the wavelengths $L_{g,i}$: 628.32 and 62.832 and to the frequencies f_i: $1.130 * 10^{-3}$ Hz and $1.130 * 10^{-2}$ Hz . The initial conditions are set in the following tables 6 and 7. The Reynolds number

per meter is $11649093m^{-1}$ and the dynamic pressure q is $19.232kPa$.

Mach	C_L	Altitude (m)	α (°)	T(K)
0.6	0.3	2330	0.593	273

Table 6: Initial conditions

Gust type	Propagation Velocity	α_g
cosine	0.6	$+1°$

Table 7: Gust characteristics

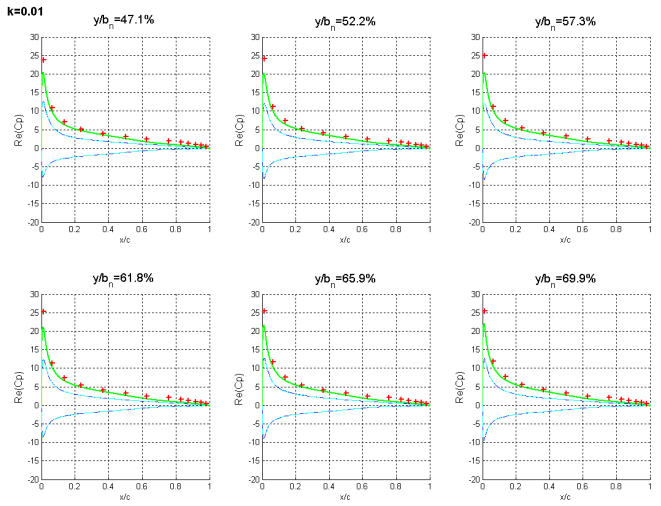

a-) Real part of the pressure coefficient

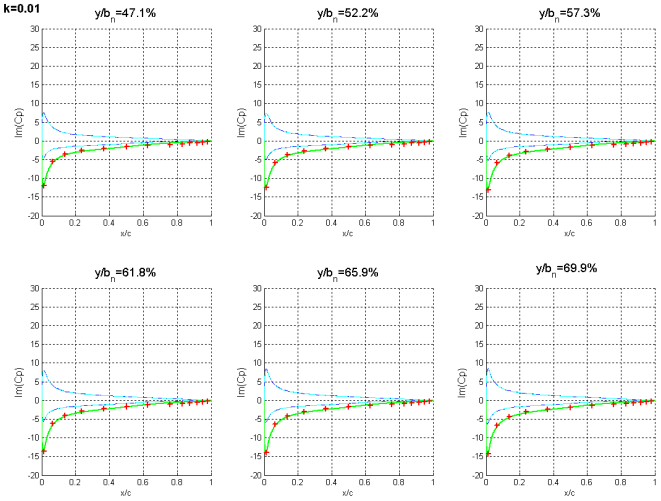

b-) Imaginary part of the pressure coefficient

Figure 11: Comparison between CFD and DLM data for a reduced frequency $k = 0.010$

In figure 11, the chosen reduced frequency is $k = 0.010$. The corresponding gust wavelength is $L_{g,i} = 628.32$ which corresponds to 54.6 times the characteristic length of the wing $L_{ref} = 11.507$. The value b_n is the half wing span, y is the position of the cut from the middle of the fuselage, and the C_p distributions on the cross sections are plotted in the following figures. Six cross sections are studied here and are respectively located at 47.1%, 52.2%, 57.3%, 61.8%, 65.9% and 69.9% of the wing half span. In order to have an accurate comparison between the DLM and the CFD, the cross sectional area have to be not to close to the fuselage or to the wing tip where some characteristical phenomena, as vortices, may influence the airflow and thus the C_p.

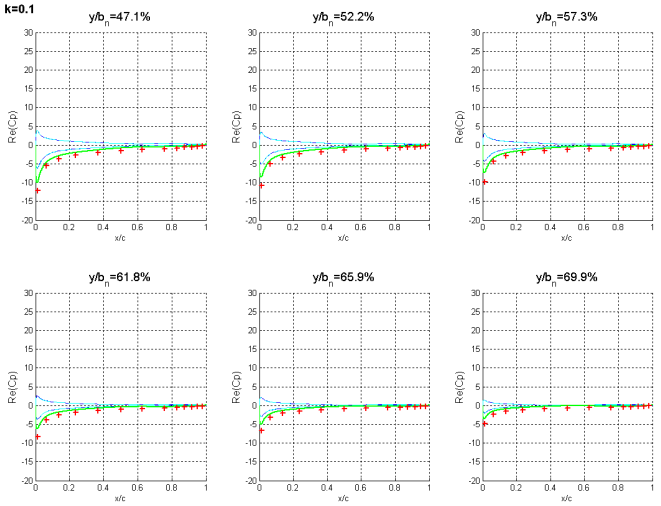

a-) Real part of the pressure coefficient

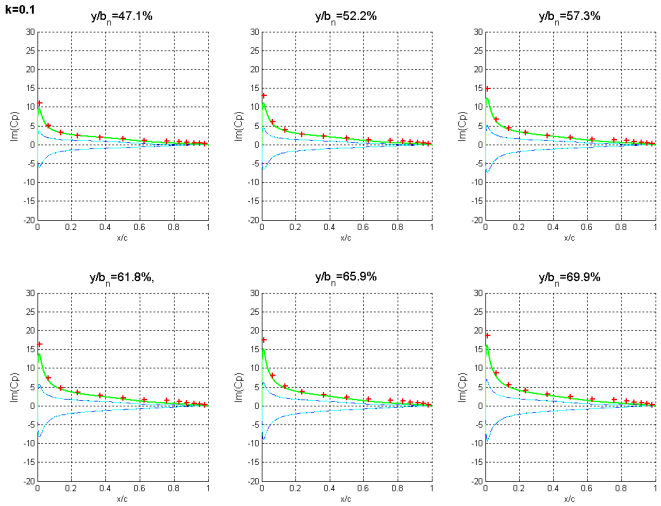

b-) Imaginary part of the pressure coefficient

Figure 12: Comparison between CFD and DLM data for a reduced frequency $k = 0.10$

In figure 12, the chosen reduced frequency is $k = 0.10$. The frequency is higher which gives a smaller gust wavelength $L_{g,i} = 62.832$ which is only 5.5 times the characteristic wavelength. Usually the design department uses gust simulations with a wavelength of 12.5 times the chord in order to perform validations. Thus, the wavelength is here less than half this value and infinitesimal differences may be seen between CFD and DLM. Nevertheless the results are closed and the margins are acceptable and are in the standard margin required for validation.

2.4 Chimera Simulations

The results from the steady computation are shown in terms of pressure coefficient distribution in the following figure 13 for two aileron configurations.

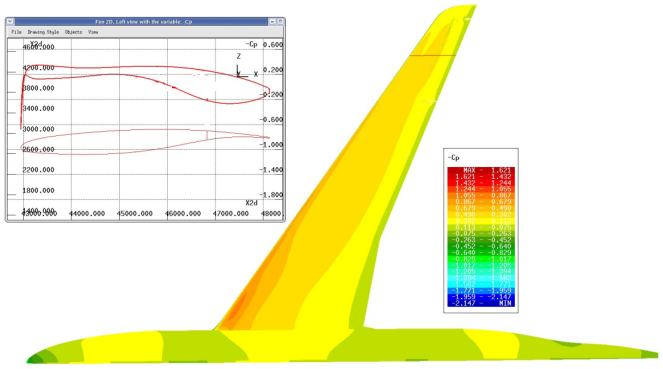

a-) C_p distribution on the HiReTT configuration with aileron [0° deflection]

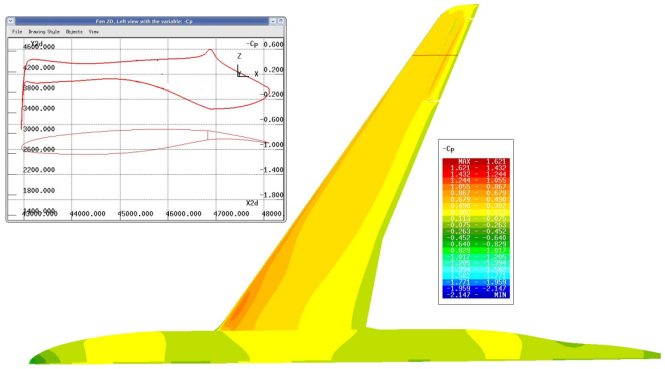

b-) C_p distribution on the HiReTT configuration with aileron [+5° deflection]

Figure 13: Pressure distribution for Chimera simulations in steady flow with two aileron configurations

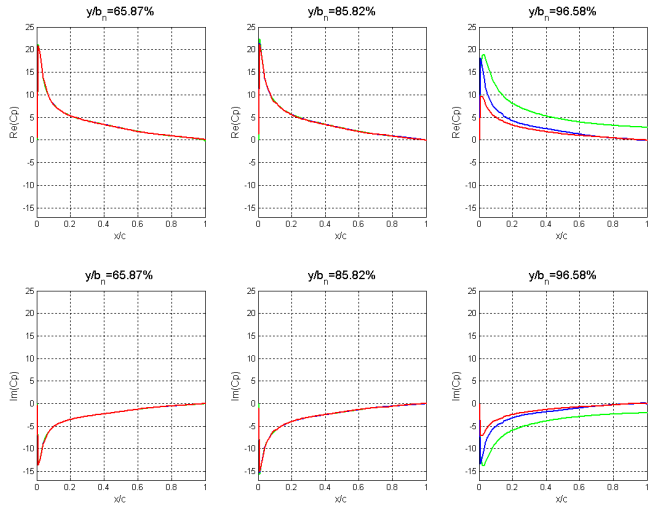

Figure 14: Real and Imaginary part of the pressure coefficient at different location for $k = 0.01$ (delta value between the upper and the lower wing)

For subsonic computations, the values in $\Delta Re(C_p)$ and $\Delta Im(C_p)$ are compared. The aerodynamic flow is studied around a clean configuration (without aileron), and chimera simulations are performed with +0° and +5° aileron positions. Figure 14 shows the evolution of the real and imaginary parts of the pressure coefficient C_p. These unsteady simulations are performed in subsonic flows and no differences between the curves are highlighted for a position on the wing before the aileron ($y/b_n = 65.87\%$) or on the aileron ($y/b_n = 85.82\%$). The differences highlighted for a position after the aileron ($y/b_n = 96.58\%$) is due to wing tip effects. In this section, the wing tip is curved and some complex aerodynamic phenomenon appears. For this reason of similarities, the differences between the results from the configuration with aileron and the clean configurations are plotted at two locations in figures 15 and 16.

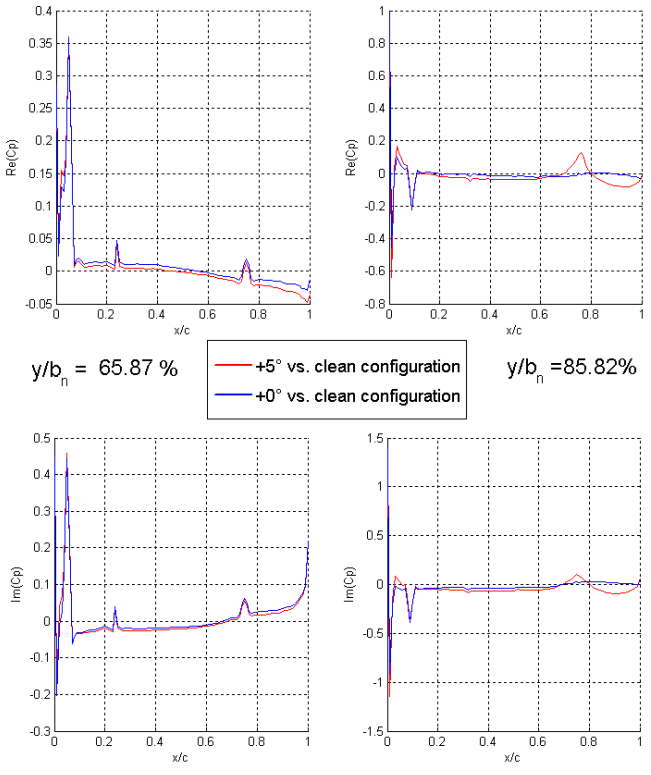

Results for k=0.01

Figure 15: Differences between HiReTT configuration with aileron and clean one in term of $\Delta Re(C_p)$ and $\Delta Im(C_p)$

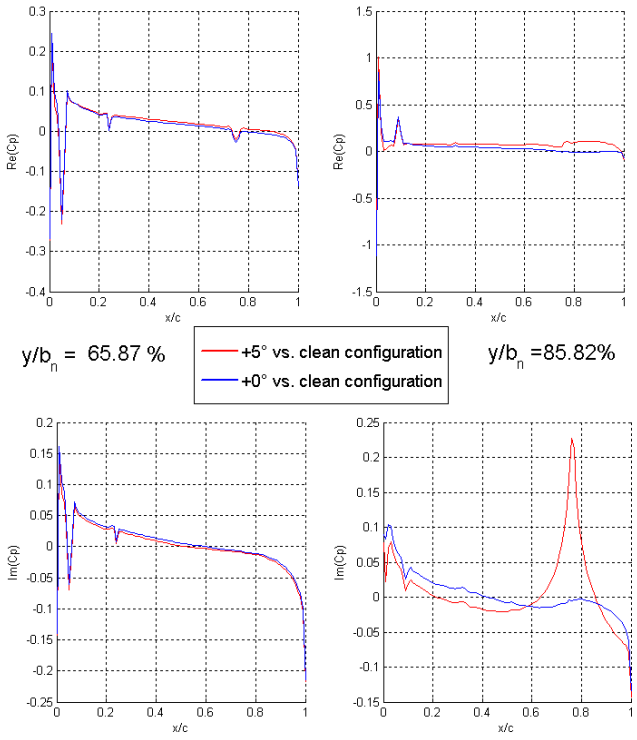

Results for k=0.01

Figure 16: Differences between HiReTT configuration with aileron and clean one in term of $\Delta Re(C_p)$ and $\Delta Im(C_p)$

3 Discussion

3.1 A linear gust response for small gust velocities

Aerodynamics gust response problem may be non-linear. The unsteady simulations performed on the NACA64A10 airfoil profile and on the HiReTT configuration have shown that the response is linear with the gust velocity when α_g stays in the interval $[0°, 3°]$. This linear relation allows the extrapolation of the different simulations and ensure the gust validation from non linear effects to to the gust amplitude. Today, there is a need to perform calculations also for higher angles. It will be very useful to perform research on the gust response outside these boundaries in order to have more possibilities in the load simulations.

3.2 A dynamic response to compute loads

The dynamic response of the different configurations have been studied and films have been created to look at the displacement. The results were in agreement with the harmonic excitation. The dynamic response is fundamental when the aeroelastic design is performed. The loads drive the aeroaelatic phenomena and have to be computed all along the development of the aircraft. With these simulations, it has been shown that static and dynamic motions are assessable for gust response in URANS simulations.

3.3 A validated gust model

The CFD results are in agreement with the DLM results given by the aeroelasticity department. As the figure 8 shows, the red crosses match pretty well with the green curves. Some differences come from the approximations done when DLM are used.

In transonic region, some parts of the airflow over the wing become supersonic. For simulations at Mach 0.8, an abrupt change in pressure distribution appears, it is due to the formation of a shock wave. Two shocks appear, one on each parts of the wing as figure 17 shows.

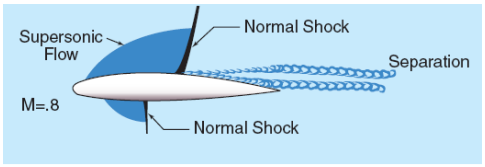

Figure 17: Shock waves in transonic regime (from [6])

Figure 9 shows the apparition of shock waves on the wing surface around the mid-chord since the blue curve features a peak value. Here a delta is shown and for some frequencies, shock waves may appear at the same location on the lower and upper wing which gives small values in $\Delta Re(C_p)$ and $\Delta Im(C_p)$. Concerning forced motion, some non linear phenomena appear at high reduced frequencies. The DLM cannot simulate these flow patterns accurately and differences in the comparison are highlighted in figure 10.

To conclude, both for the NACA64A10 wing profile and for the HiReTT configuration, the comparison between CFD and DLM gives acceptable results and allows the gust model validation for these types of configuration. These two models are validated and thus the method can be applied for more complex configurations as an industrial aircraft.

3.4 An application of the gust response: Chimera simulations

Figure 14 highlights only negligible differences. This is a normal pattern for this type of simulations in subsonic flow. Nevertheless, for computations in transonic flow, differences will appear due to shocks waves, buffet, etc. The same types of results are obtained for a higher reduced frequency (k=0.1 for example).

These Chimera simulations have been computed essentially to see if the simulation is possible for this type of industrial configuration. The results show that this is the case. Thus, gust simulation can be performed.

3.5 A post-processing to improve

Post-processing takes a long time today for these simulations. No tool exists for automatic post processing.

In this paper, all the results presented come from a post processing with MATLAB, ens++, quickview or small fortran scripts. For the future, work on post-processing is essential in order to use this model in industrial applications.

Conclusion

The main objective of this work was to get a new tool for gust response simulation in Computational Fluid Dynamics (CFD). The classical used methods are efficient only for subsonic flows and do not take into account turbulent flows or body thickness effects due to the assumptions done with the Doublet Lattice Methods (DLM).

U-RANS simulations have been performed on several meshes in order to determine the compatibility of the gust model with unsteady simulations in elsA.

In a first time, tests have been performed on a wing profile airfoil: the NACA64A10, in order to look for the response of the structure to a gust perturbation in a simple case. Nondimensionalization, gust wavelength, gust velocity and other parameters have been tested as input to see their influence on the results and to know how they could be used in order to perform gust simulations in CFD. In the same way, the gust response of the rigid HiReTT configuration (A380 wing/body configuration) has been tested in static. Then, dynamic motion has been performed and it has been shown that gust simulations are working for dynamic coupling methods (direct simulations of the fluid/structure interactions).

In a second time, a harmonic gust excitation has been used in order to perform gust simulations on 2D and 3D configurations and to compare the results to the DLM used in most of the departments for gust loads calculations. The first harmonic of Navier Stokes unsteady simulations has been compared with the DLM one. The performed simulations have shown that the gust model used in CFD gives the same results than the DLM for different frequencies and wavelengths. The results are coherent for the tested range of velocities, for subsonic flows, with the actual industrial methods used in Airbus. The possibility to simulate even at low or high frequencies has been shown as well as for transonic flows.

Finally, Chimera simulations have been done in order to look for the applicability of the method on industrial configurations. This industrial application is a wing/aileron/body configuration. The work has proven that gust response for unsteady simulations can be performed on complex configurations and gives coherent results.

All these results present several interesting perspectives for the development of the gust response simulation in CFD and the loads calculation. The future studies on these simulations should focus on possible post-processing ways. In particular, needed output data should be defined by the different departments. In this report, all the post processing has been done with ens++, quickview and MATLAB. This task takes a long time in the gust response studies and should be automated before the use of these methods in the Airbus industrial framework. The fluid structure interaction simulations for higher gust amplitudes should be also investigated.

Acknowledgments

I would like to gratefully acknowledge my supervisor Julien DELBOVE for the support provided all along these months, for his patience, for answering all the different questions I have had and for his attention to the researches made during this thesis.

I want to express my gratitude to the reviewers for their suggestions and comments and particularly to my KTH tutor David Eller who has followed my work during this thesis. It is also a pleasure to thanks Christophe POETSCH for having provided support to this master thesis with the DLM simulations. I would like to thanks the others master thesis students (Amandine R., Adrià V., Jérôme V., Pierre-Jean B., and Thomas P.) which made these months joyful.

Finally I wish to thank all the engineers in the EGAMT2 technical team, Pascal LARRIEU and Jerôme BOSC the managers.

References

[1] Onera. Design and implementation tutorial. http://elsa.onera.fr/ExternDocs/user/MDEV-06001.pdf, 2006. [Online].

[2] Julien Delbove. *Contribution aux outils de simulation aéroélastique des aéronefs: Prediction du flottement et deformation statique des voilures.* PhD thesis, Supaero, 2005.

[3] Toni El-Dirani. Fidelity of flight control systems in a real-time optimal trajectory planner. Master's thesis, Massachusetts Institute of Technology, 1990.

[4] K.C. Hall J.P. Thomas and E.H. Dowell. Reduced-order aeroelastic modeling using proper-orthogonal decompositions. Technical report, 2010.

[5] Frederic M.Hoblit. *Gust loads on aircraft: Concepts and applications.* Education Series, 1988.

[6] U.S. Federal Aviation Administration. *Airplane Flying Handbook (FAA-8083-3A).* U.S. Government Printing Office, 2004.

[7] Ignacio Gonzalez Martino. Unsteady simulations in elsa: Validation of several new features for aeroelasticity. Master's thesis, ISAE Supaero, 2010.

[8] Jonathan E. Cooper Jan R. Wright. *Introduction to aircraft aeroelasticity and loads.* Wiley, 2007.

Appendix

A Results for rigid simulations

A.1 NACA64A10 airfoil profile

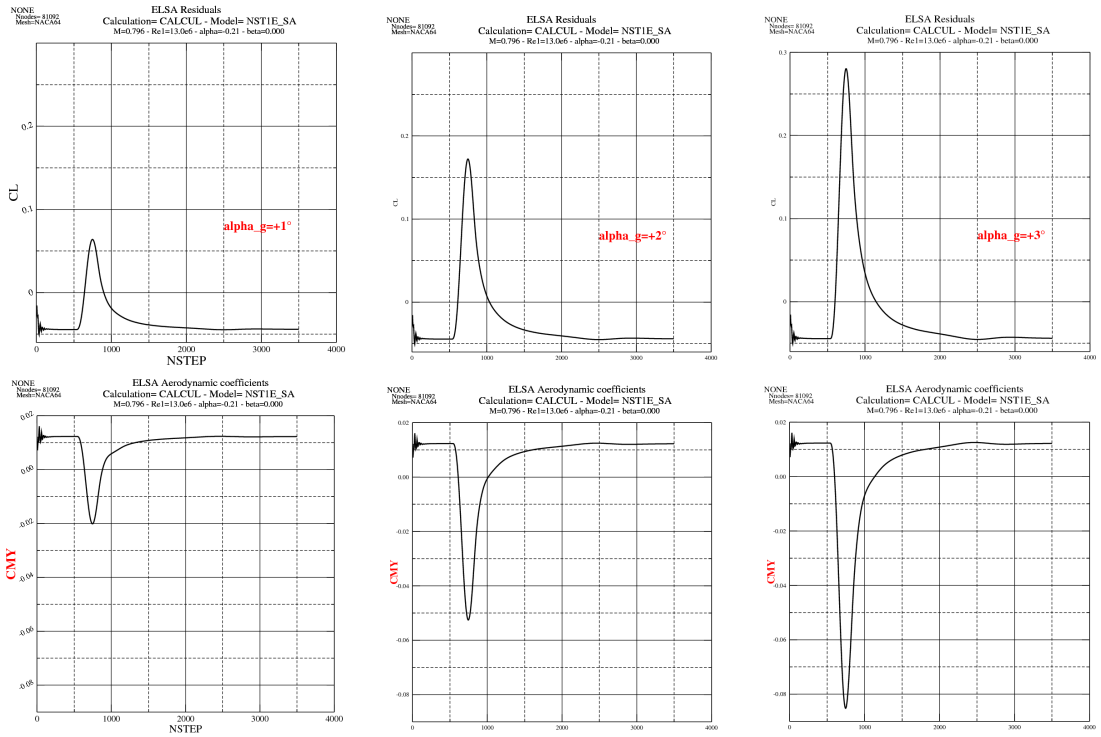

Figure 18: Lift and moment coefficients, "$1 - cos$" discrete gust response (impact of wavelength)

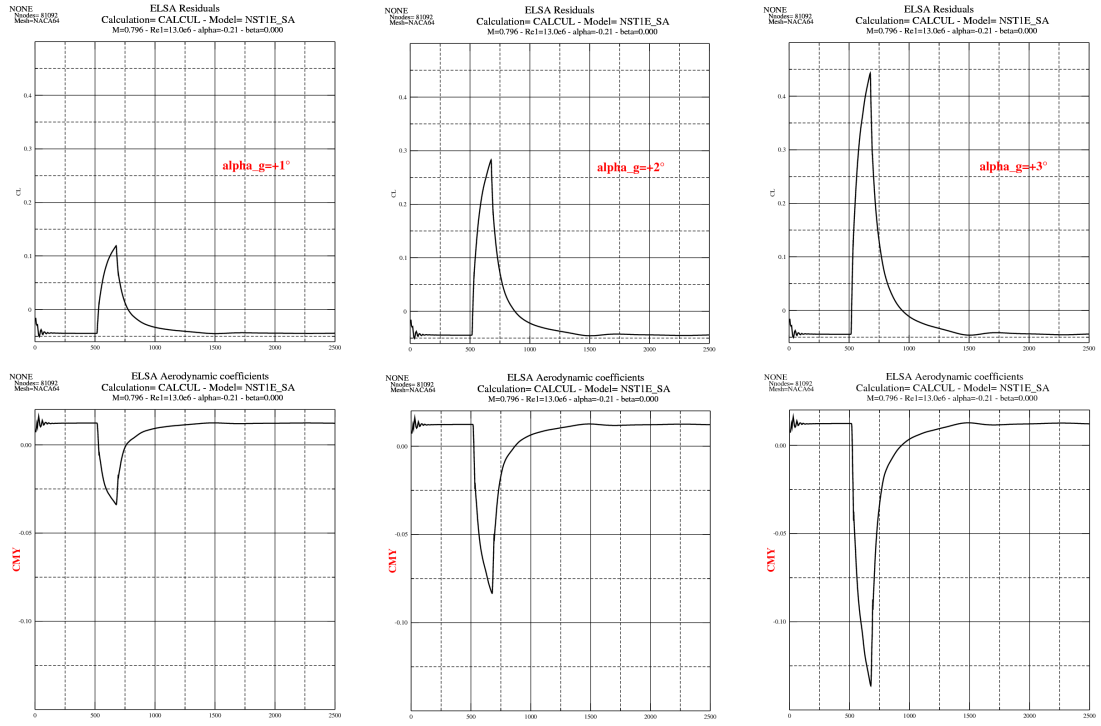

Figure 19: Lift and moment coefficients, "$sharp - edged$" gust response (impact of wavelength)

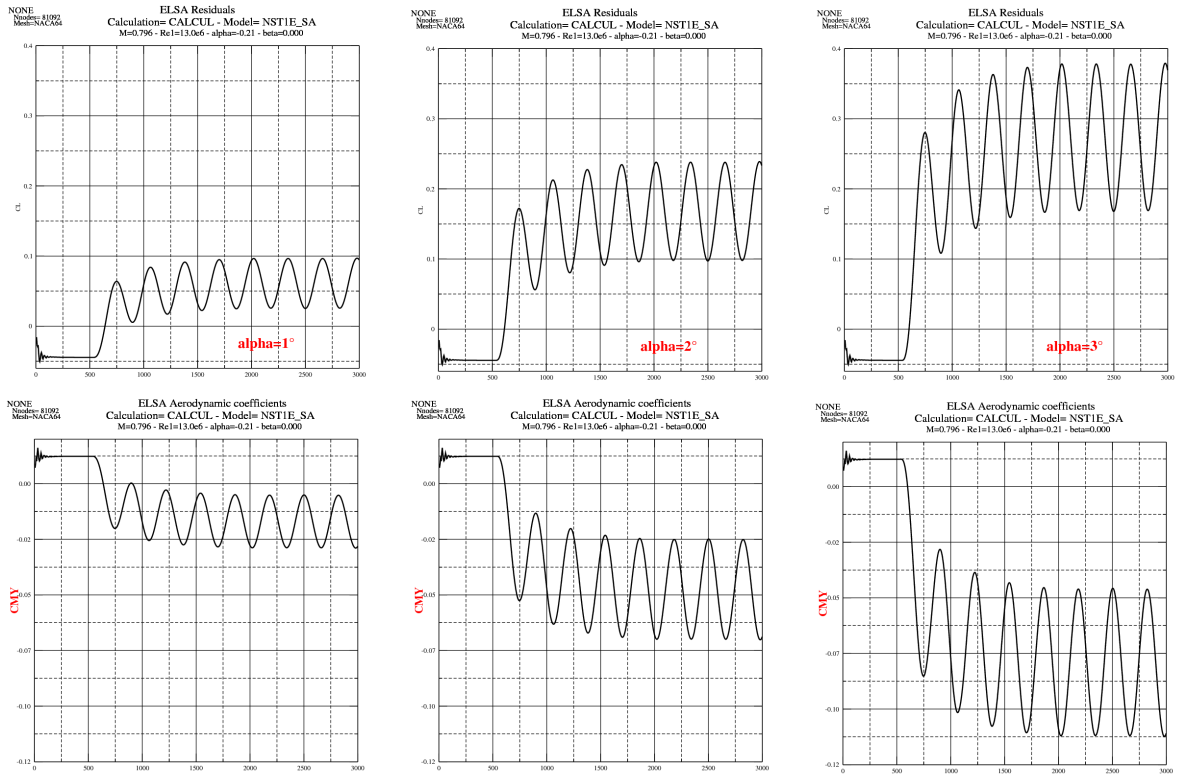

Figure 20: Lift and moment coefficients, harmonic gust response (impact of wavelength)

A.2 HiReTT configuration

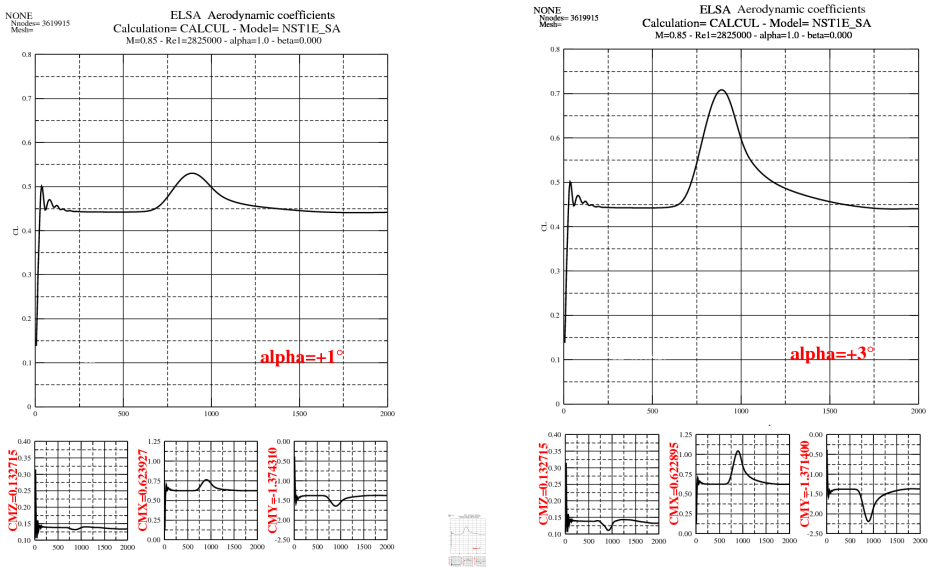

Figure 21: Lift and moment coefficients, "$1 - cos$" discrete gust response (impact of wavelength)

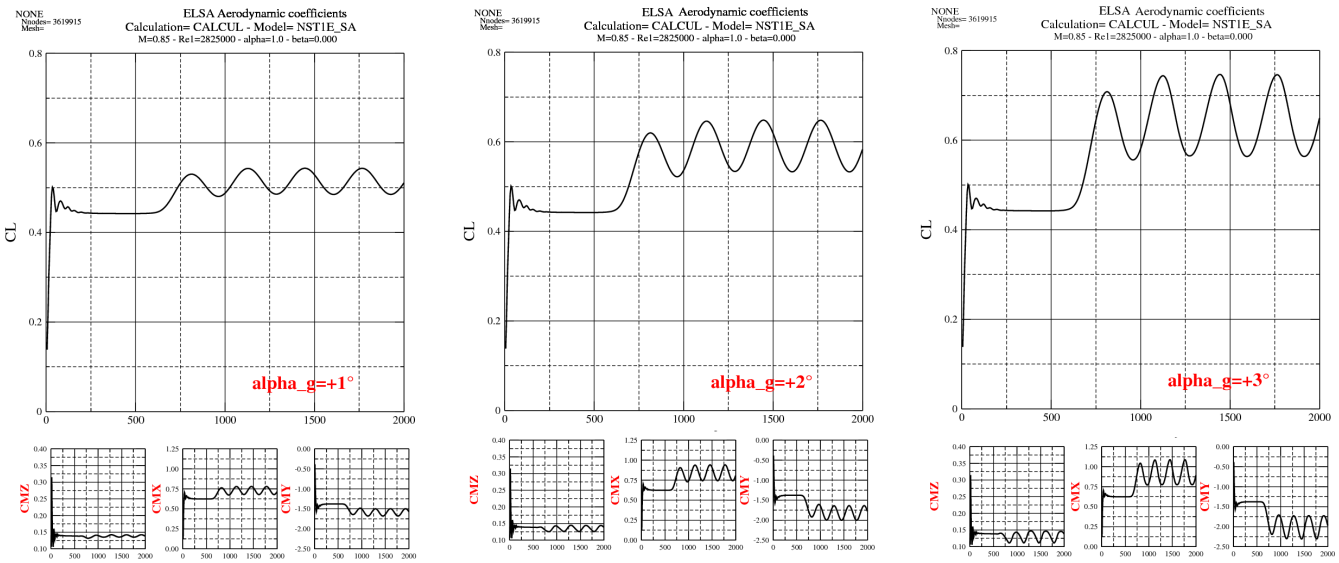

Figure 22: Lift and moment coefficients, harmonic gust response (impact of wavelength)

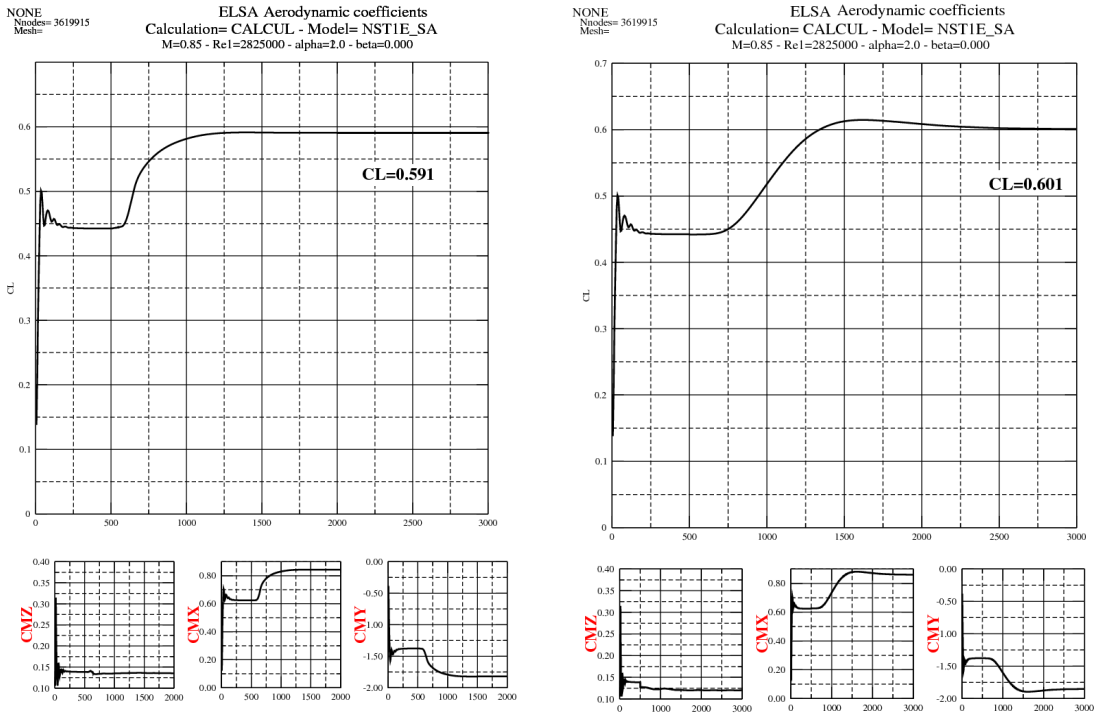

a - Sharp Edged gust response *b - Change in angle of attack*

Figure 23: Lift and moment coefficients. Comparison.

B Comparison between DLM and CFD

B.1 NACA64A10 airfoil profile

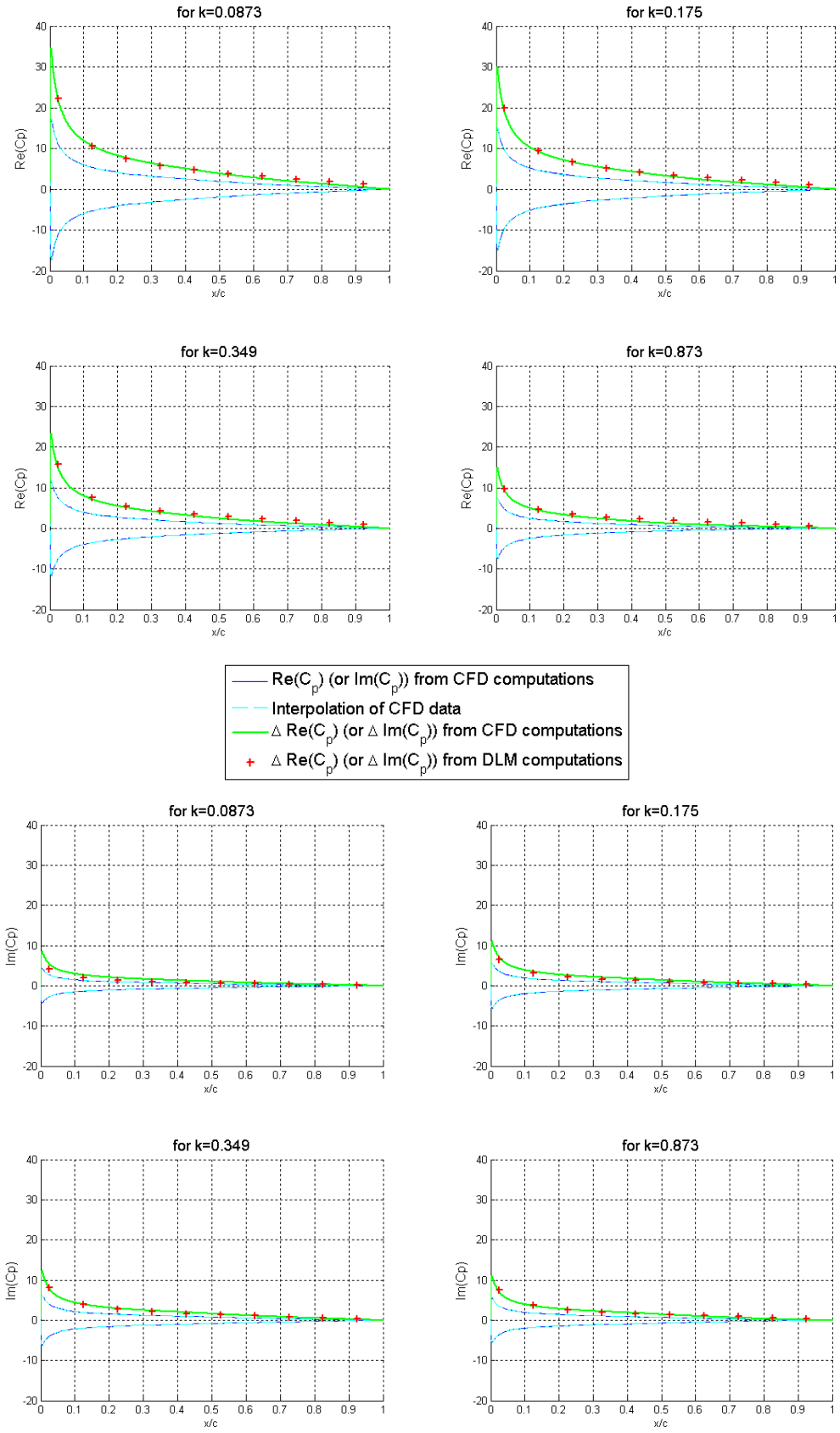

Figure 24: Comparison between CFD and DLM data for $Ma = 0.5$ (gust response)

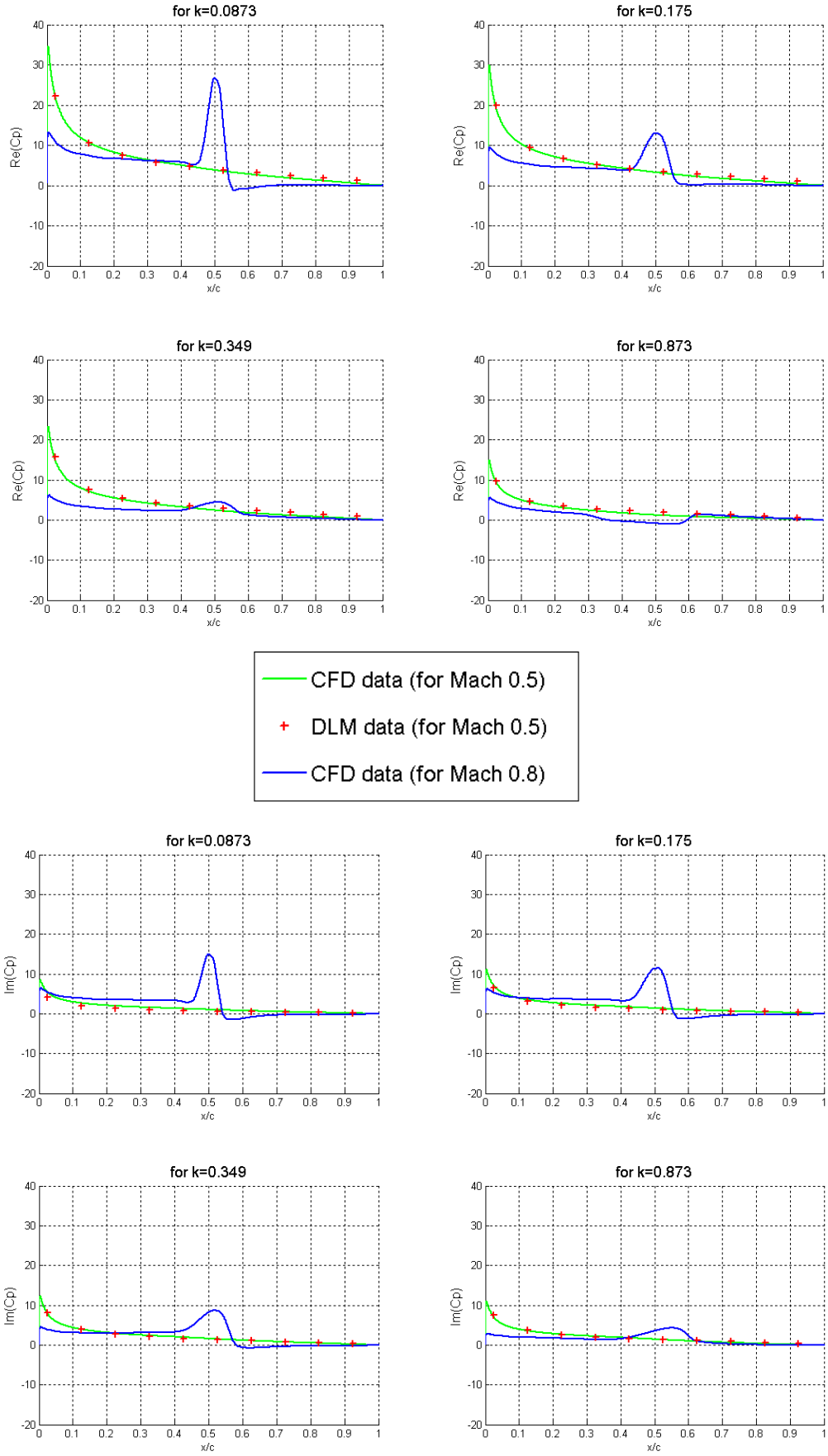

Figure 25: Comparison between two different mach numbers for CFD computations

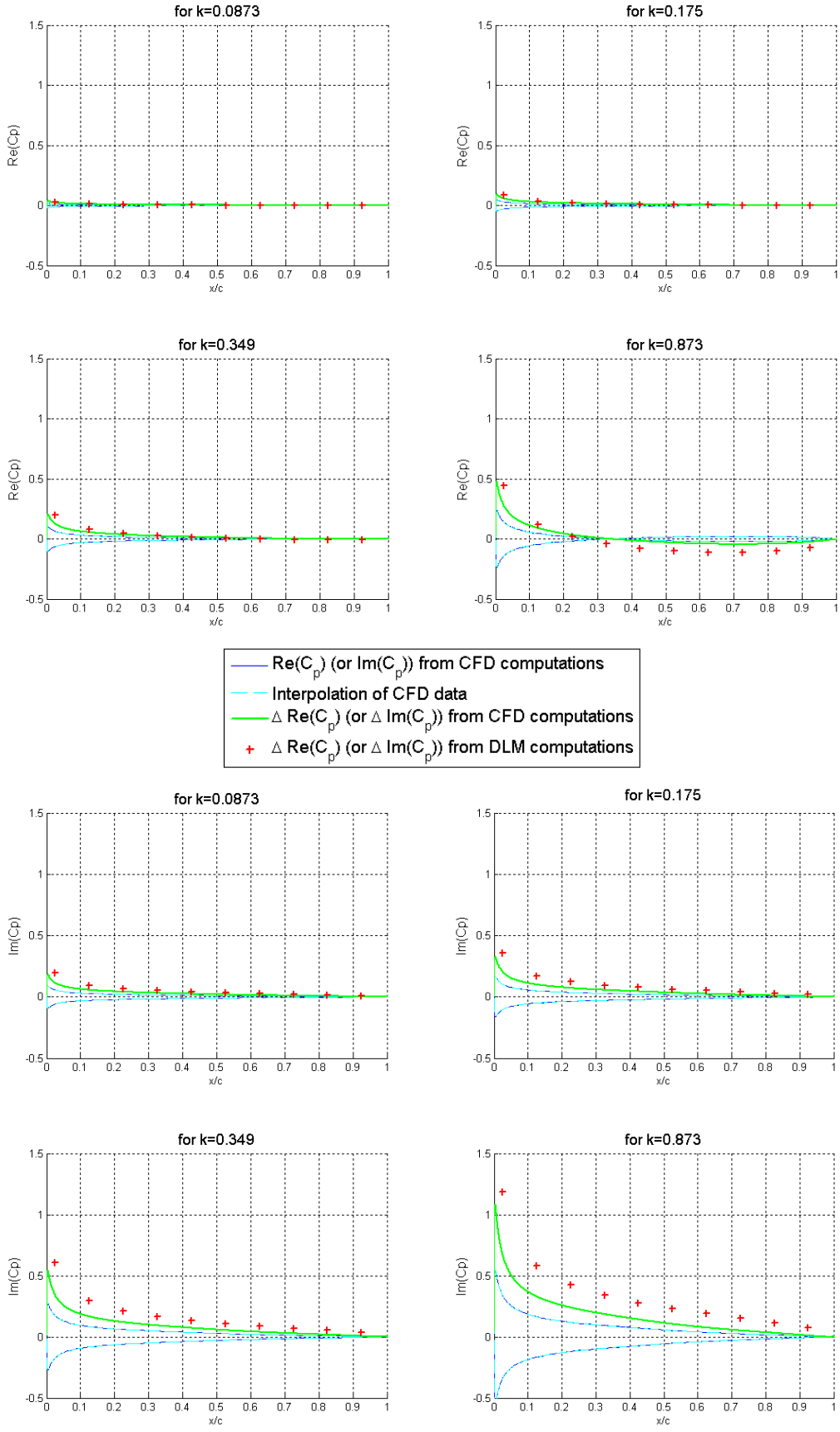

Figure 26: Comparison between CFD and DLM in forced motion ($Ma = 0.5$)

B.2 HiReTT configuration

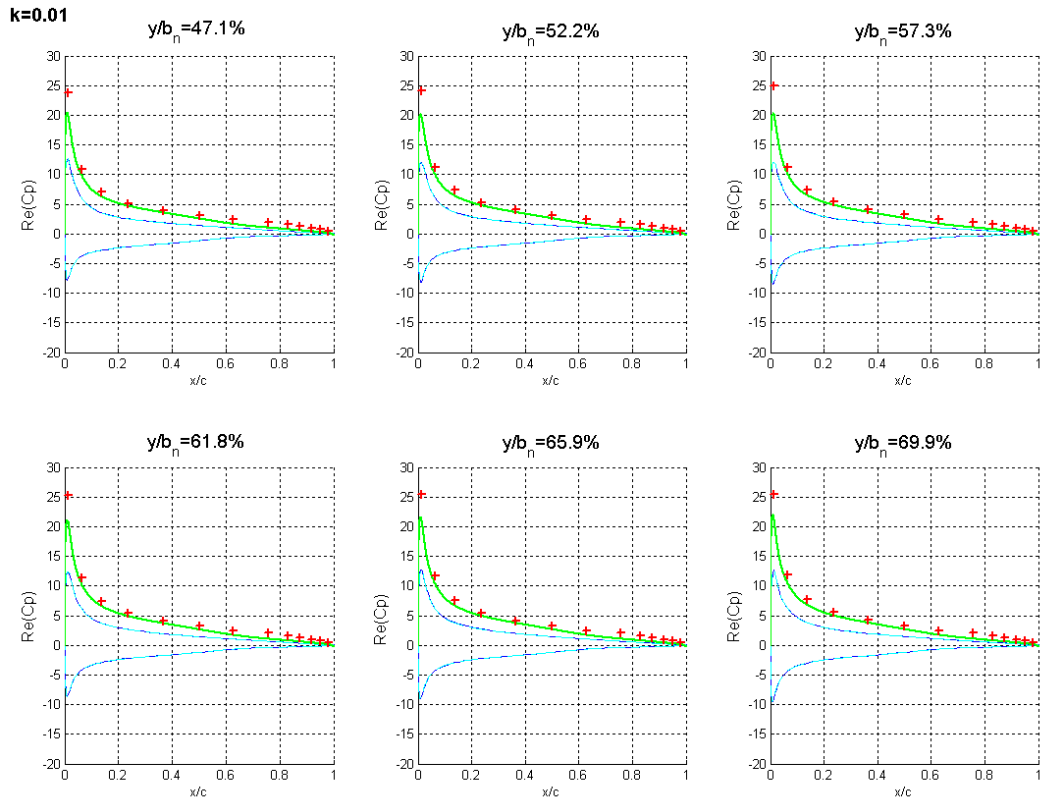

a-) Real part of the pressure coefficient

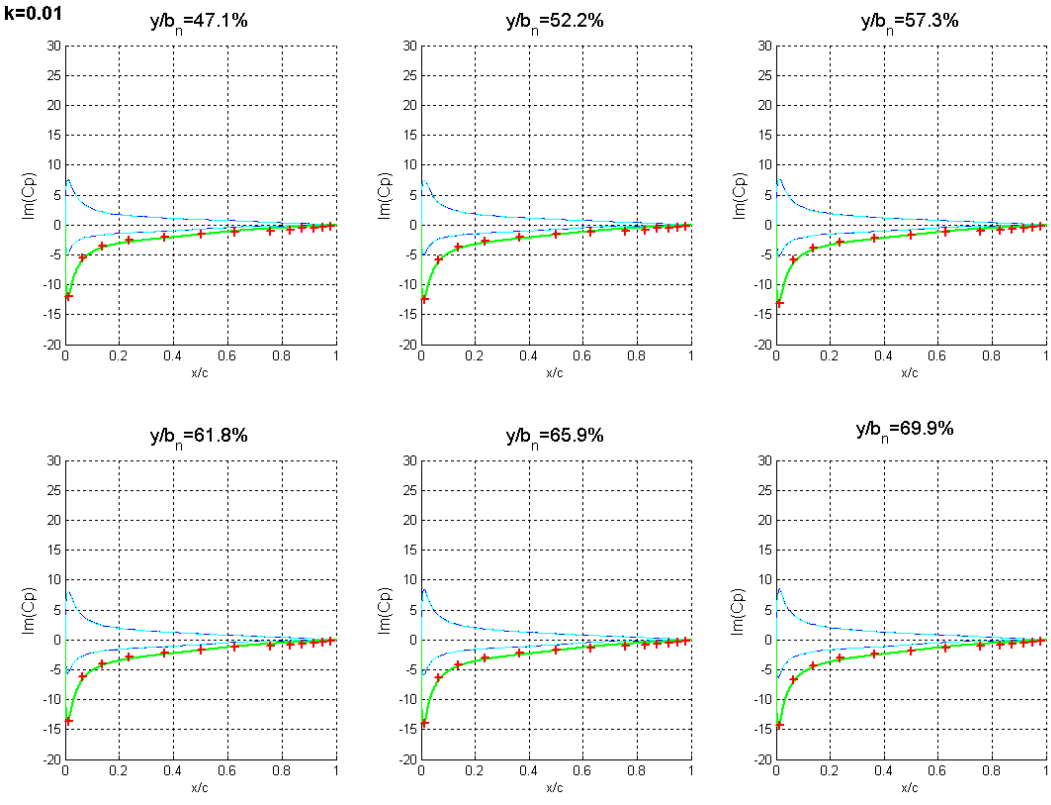

b-) Imaginary part of the pressure coefficient

Figure 27: Comparison between CFD and DLM data for a reduced frequency $k = 0.010$

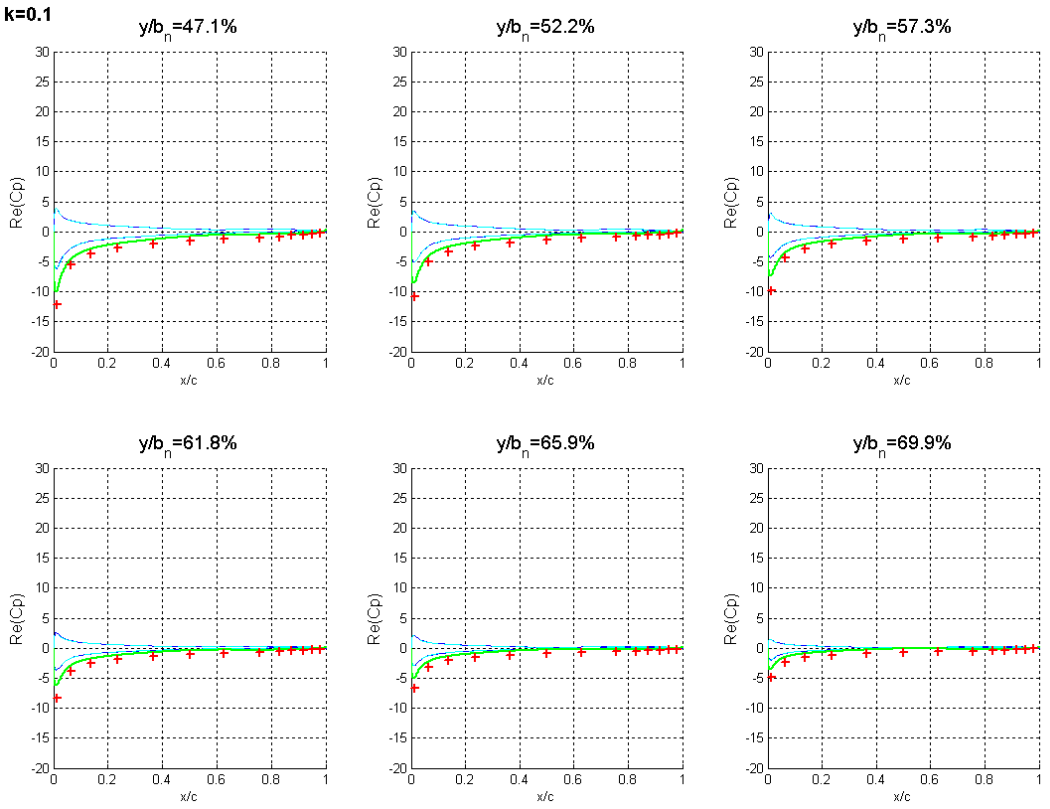

a-) Real part of the pressure coefficient

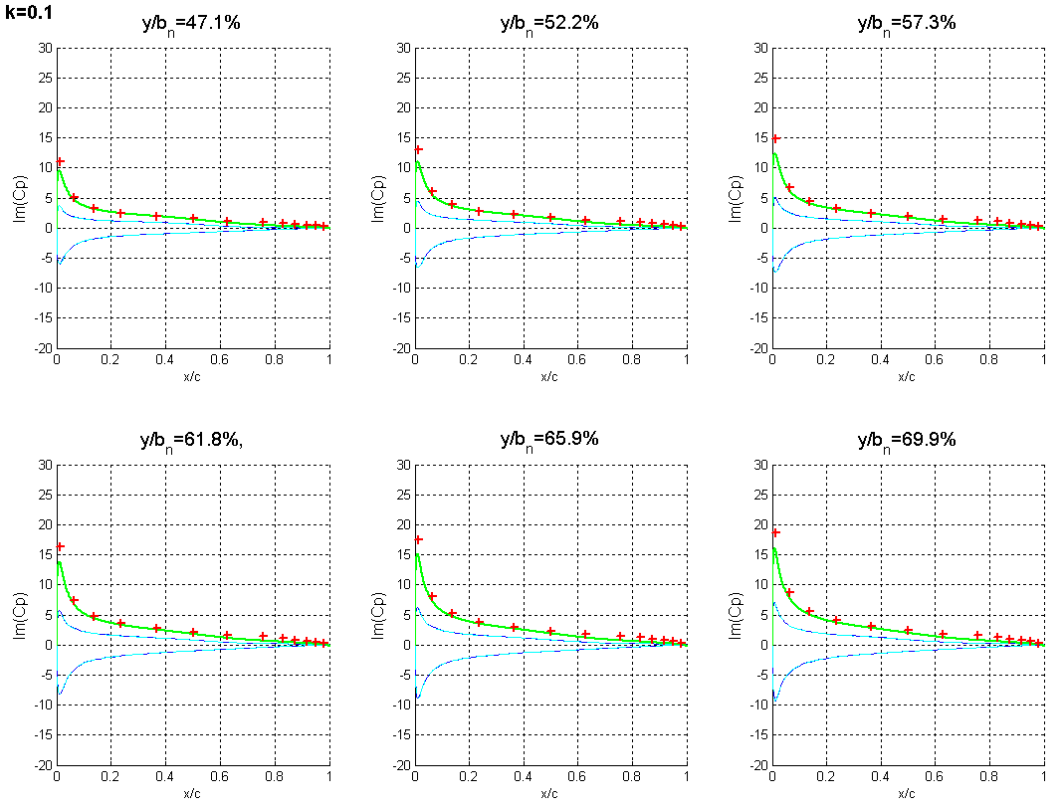

b-) Imaginary part of the pressure coefficient

Figure 28: Comparison between CFD and DLM data for a reduced frequency $k = 0.10$